ARL-TR-95-32

Copy No. _____

Scattering of a Transient Plane Compression Wave by a Spherical Inclusion in a Biot Medium

Final Report under Contract N00039-91-C-0082,
TD No. 01A2081, Buried Target Detection Model

Dennis J. Yelton
Morris Stern
Hans G. Schantz

Applied Research Laboratories
The University of Texas at Austin
P. O. Box 8029 Austin, TX 78713-8029

26 October 1995

Final Report

21 June 1994 - 30 June 1995

Approved for public release;
distribution is unlimited.

Prepared for:
Naval Research Laboratory
Stennis Space Center, MS 39529-5004

Monitored by:
Space and Naval Warfare Systems Command
Department of the Navy
Arlington, VA 22245-5200

This page intentionally left blank.

TABLE OF CONTENTS

This page intentionally left blank.

LIST OF FIGURES

This page intentionally left blank.

PREFACE

This report is the final report on work tasked to Applied Research Laboratories, The University of Texas at Austin (ARL:UT) under Contract N00039-91-C-0082, TD No. 01A2081, entitled Buried Target Detection Model.

This page intentionally left blank.

1. OBJECTIVE

The goal of this study is to develop accurate computational techniques for modeling acoustic scattering from a target embedded in a two-phase poroelastic medium, such as a water-filled sandy sediment. Such modeling capabilities would substantially enhance existing sonar performance prediction models.

Previous tasks, ending with TD No. 01A1038, demonstrated the penetration of significant acoustic energy into sandy sediments at shallow grazing angles. This phenomenon has potentially important consequences when applied to the detection and classification of buried targets. It opens the door to the possibility of using active sonar backscattering to detect and categorize buried objects at long range. However, this possibility can only be realized if the capacity to accurately model acoustic penetration and scattering is well developed.

Contrary to experimental observations, current elastic medium propagation models such as SAFARI and PE are unable to account for acoustic penetration at shallow grazing angles. This is an inherent limitation of elastic sediment models. For a given frequency, these models predict the existence of one, and only one, acoustic compression wave within the sediment. For smooth surfaces, model parameters that are compatible with observed values of sediment acoustic wave speed and attenuation inevitably predict a critical grazing angle, below which negligible acoustic energy penetrates the sediment.

Experimental measurements also indicate the existence of a second acoustic wave in water-saturated sand. Therefore, a model that can accommodate two acoustic waves is required. One such model is Biot's theory of acoustic propagation in poroelastic media, which predicts the existence of both a fast and a slow acoustic compression wave. Model parameters that match the fast wave speed with observed values predict a critical grazing angle for the fast wave, but not necessarily for the slow wave. Thus, acoustic energy can penetrate into the sediment at any grazing angle.

This study explores the effectiveness of Biot's theory in modeling acoustic scattering from spherical targets embedded in a sandy sediment. If extended

testing proves Biot's theory to be reliable, the ultimate goal is to combine this scattering model with an acoustic propagation and penetration model, producing a fully integrated target detection scheme for targets buried in sandy sediments.

2. INTRODUCTION

Over the years, the ocean sediment has been modeled as a fluid, elastic solid, and most recently as a fluid-filled poroelastic solid.[1-3] Although these models make similar predictions in some respects, there are notable differences. Perhaps the most significant is the number and types of wave disturbances each type of medium will support. Fluid media support a single compression wave, elastic media support one compression wave and one shear wave, and poro-elastic media support two compression waves and one shear wave. The indices of refraction and scattering properties of these different waves can vary considerably. The three models result in decidedly different scenarios for the detection of objects buried within the seabed. This is especially true for waves incident on a smooth seafloor at shallow grazing angles.

Recent analysis of experimental bottom penetration results by Chotiros[4-6] is consistent with the poroelastic theory developed by Biot.[7,8] Thus it seems reasonable to apply Biot's theory to model scattering from an inclusion within the sediment. Indeed, a few approaches to this problem have already been investigated. In the long wavelength limit, analytic expressions were obtained by Berryman[9] for scattering from a spherical elastic inhomogeneity within a Biot medium. More recently, Kargi and Lim[10] developed a transition matrix technique and applied it numerically to scattering from a spherical Biot inhomogeneity within a Biot medium. But the most general treatment to date was given by Zimmerman and Stern,[11] who derived a series solution for the scattering of plane compression waves by a fluid, elastic, or rigid spherical inclusion within a Biot medium.

The numerical results presented here are based on the work of Zimmerman and Stern. The incident wave can be composed of any linear combination of Biot fast and slow compression waves. Also, the scattered wave is easily decomposed into its fast, slow, and shear components. The angular dependence of the scattered fast and slow components is investigated, and compared with experimental results.

This page intentionally left blank.

3. MODEL

Biot's theory predicts acoustic propagation through a poroelastic medium as a coupled wave motion within the solid and the pore fluid. The medium is modeled as a solid with tubular pores, as illustrated in Fig. 3.1. The propagating wave, in the direction of the pore tubes, can be decomposed into three components -- fast and slow compression waves, and a shear wave. The equations of motion, in a form used by Zimmerman and Stern,[11] are

$$\nabla \cdot \sigma_s + \mathbf{B}_s - b\frac{\partial}{\partial t}(\mathbf{U} - \mathbf{V}) = \frac{\partial^2}{\partial t^2}(\rho_{11}\mathbf{U} + \rho_{12}\mathbf{V}) \qquad (3.1)$$

and

$$\nabla s + \mathbf{B}_f + b\frac{\partial}{\partial t}(\mathbf{U} - \mathbf{V}) = \frac{\partial^2}{\partial t^2}(\rho_{12}\mathbf{U} + \rho_{22}\mathbf{V}), \qquad (3.2)$$

where **U** and **V** are the solid and fluid displacements, respectively, $\mathbf{B}_s$ and $\mathbf{B}_f$ are the body forces per unit volume of bulk material applied to the solid and fluid, respectively, b is a viscous coupling parameter relating drag force to relative solid-fluid velocity, s is the negative pore pressure times the porosity, σ_s is the solid stress tensor, and the ρ's are mass coefficients.

This work is a numerical study of the scattering of transient plane compression waves from an elastic sphere embedded in an unbounded Biot medium. The geometry of the problem is shown in Fig. 3.2. The incident wave can be any linear combination of Biot fast and slow waves. A fast Fourier transform is applied to the incident wave, and each frequency component is transformed to spherical coordinates via a Legendre polynomial / spherical Bessel function decomposition.[12] Then the steady-state solution of the above equations of motion are determined for each frequency by applying the appropriate boundary conditions at the Biot-sphere interface. The details of this solution technique were derived by Zimmerman and Stern,[11] using an approach previously applied by Ying and Truell[13] and Pao and Mow[14] for the case of a spherical object embedded in an elastic medium. The steady state

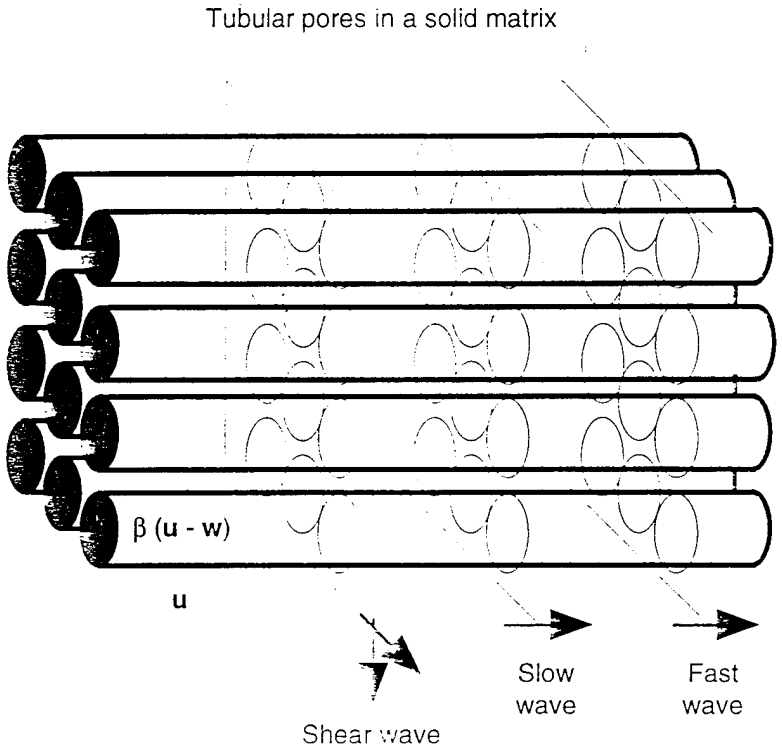

Figure 3.1
Illustration of Biot's theory of acoustic propagation through a poroelastic medium.

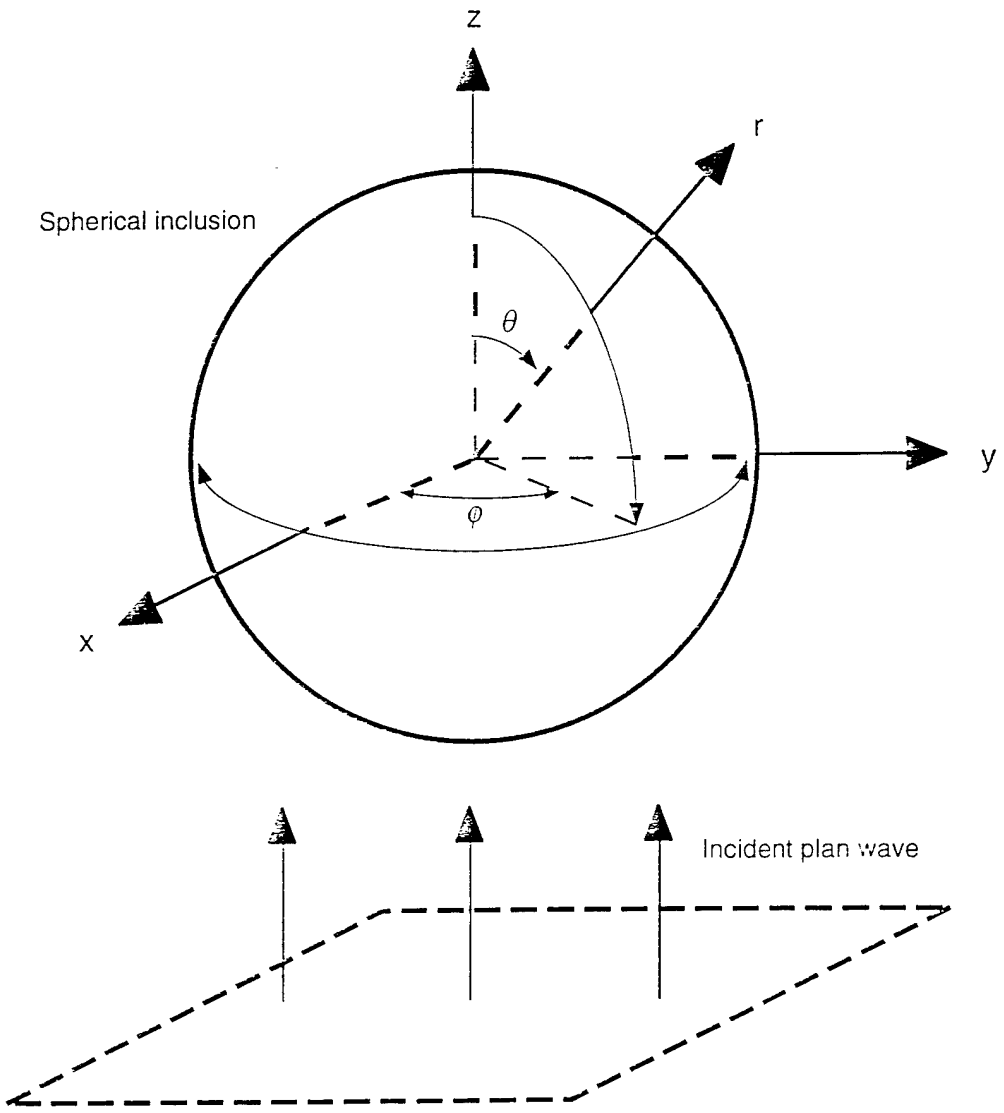

Figure 3.2
Problem geometry.

solution for each angular frequency, ω_n, is multiplied by $\exp(-i\omega_n t)$, and the results are summed to give the full transient scattered wave solution.

4. NUMERICAL IMPLEMENTATION

The numerical implementation of the series solution developed by Zimmerman and Stern was quite straightforward, although somewhat tedious. The only serious difficulties that could potentially compromise the calculations were the choice of Bessel function and Legendre polynomial routines, and the choice of a convergence criterion for the series solution. The reliability of the numerical results critically depends on the reliability of these two choices.

The Bessel function and Legendre polynomial routines used were the library of routines developed by Amos, of Sandia National Laboratories. The routines are in double precision and were used to evaluate Bessel functions of the first, second, and third kind, as well as Legendre polynomials. The routines are available on the World Wide Web at the URL "http://netlib.att.com/magic/netlib_find?db=0&pat=amos." A general overview of the routines and a discussion of their capabilities and limitations are given in the file "amos/readme."

The solution series was considered to have converged when both the incremental radial solid displacement term and the incremental radial stress term had decreased in magnitude to a point less that 10^{-5} times the series sum prior to those terms. For a 3.5 cm diam sphere, and in the frequency range from 100 kHz to 300 kHz, convergence was obtained out to a distance of four sphere diameters by using 30 terms for the incident wave series and ten terms for the scattered wave series. All the computations were done in double precision.

This page intentionally left blank.

5. NUMERICAL RESULTS

The scattering of transient plane compression waves by a 3.5 cm diam steel sphere embedded in an unbounded Biot medium was simulated numerically. The properties of the Biot medium and the steel sphere are given in Tables 5.1 and 5.2, respectively. The input was a vibrating planar surface at a distance of 10 cm from the sphere. The Fourier transform of the input vibration was modeled as a cosine half-wave in the frequency domain, in the frequency band 100-300 kHz, as shown in Fig. 5.1. Of the incident plane wave, 98% of the energy incident on the sphere was in the fast wave component, 2% in the slow wave component, and a negligible amount in the shear wave component. The angular dependence, as a function of time, of the scattered fast and slow compression waves was investigated. The results are shown in Figs. 5.2 and 5.3.

For the scattered fast wave, the specular return and the successive Rayleigh waves were found to decrease as the angle changed from 180° (backscatter) to 90°. As the angle changed from 90° to 0° (forward scatter), the specular return increased again, whereas the behavior of the Rayleigh waves was unclear. For all angles, most of the scattered energy was found to be in the specular return. The time difference between the arrival times of the specular return at different angles was consistent with refraction of the plane wave through the sphere with a longitudinal wave speed of 6001 m/s. Likewise, the time difference between the specular return and the successive Rayleigh waves was consistent with a transverse wave moving around the circumference of the sphere with a wave speed of 3208 m/s.

For the scattered slow wave, the specular return was found to increase as the angle changed from 180° to 90°, whereas the Rayleigh waves were found to decrease. From 180° to 135°, most of the scattered energy was in the first Rayleigh wave, but at all other angles it was mostly in the specular return. As the angle changed from 90° to 0°, the specular return decreased and the first Rayleigh wave decreased. The behavior of the other Rayleigh waves in this regime was unclear. The time difference between the arrival time of the specular

Table 5.1
Material properties of the simulated Biot medium.

Fluid viscosity	1.00×10^{-3} kg/m s
Fluid mass density	1000 kg/m^3
Fluid bulk modulus	2.25×10^9 Pa
Grain mass density	2650 kg/m^3
Grain bulk modulus	7.00×10^9 Pa
Frame shear modulus	2.61×10^7 Pa
Frame bulk modulus	5.30×10^9 Pa
Frame shear attenuation	1.303 dB/wavelength
Frame bulk attenuation	1.303 dB/wavelength
Frame porosity	0.44
Frame virtual mass parameter	1.636
Frame pore size parameter	3.209×10^{-4} m
Frame permeability	2.265×10^{-9} m^2

Table 5.2
Properties of the simulated steel sphere.

Diameter	3.5×10^{-2} m
Mass density	7850 kg/m^3
Longitudinal wave speed	6001 m/s
Transverse wave speed	3208 m/s

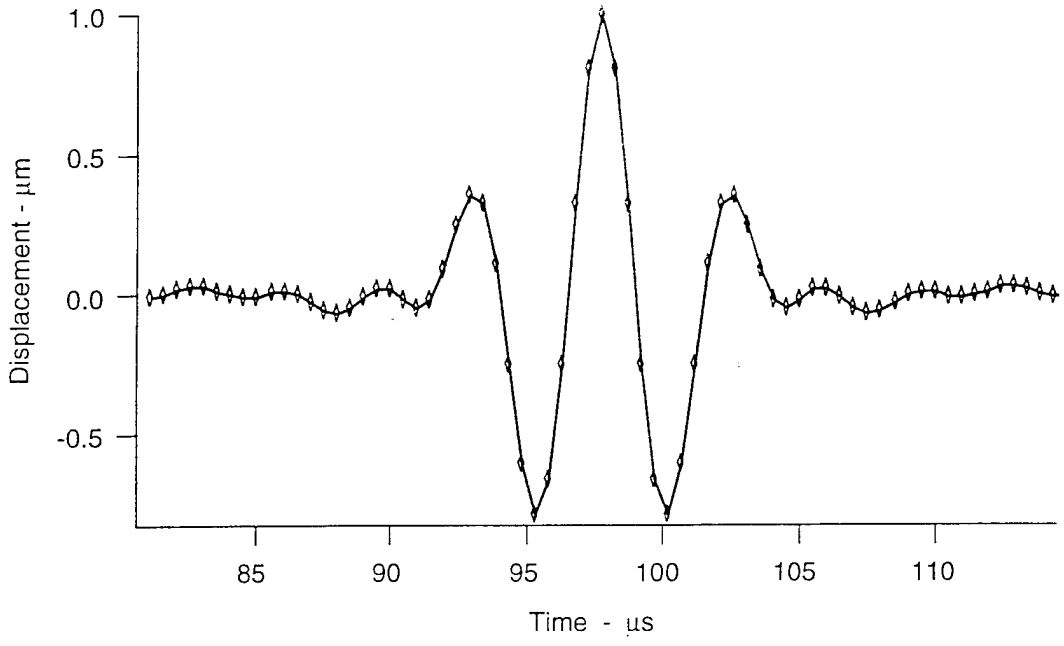

(a) Time domain

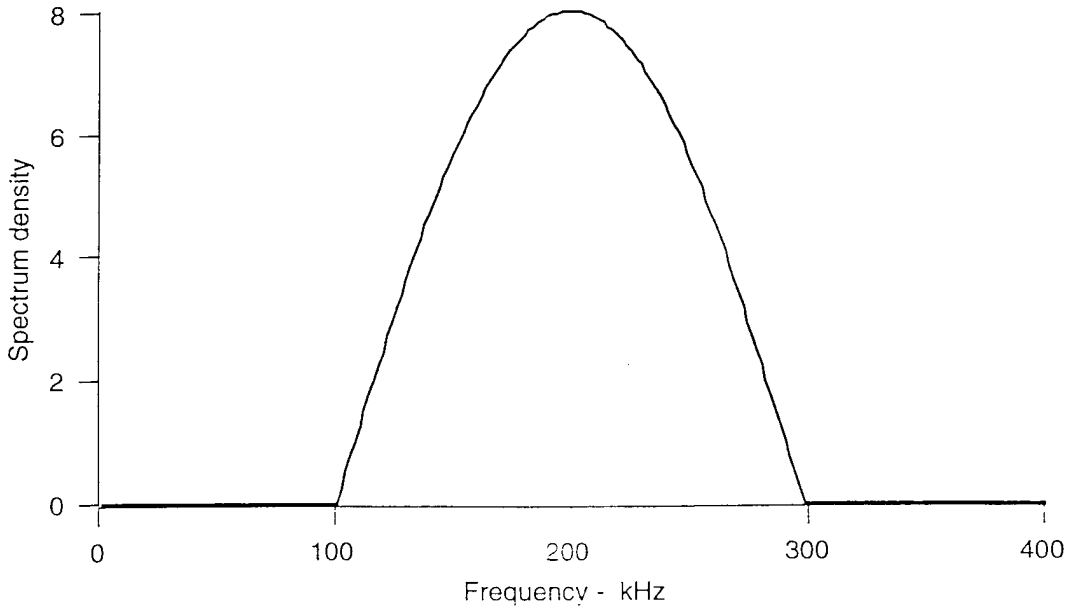

(b) Frequency domain

Figure 5.1
Incident wave at z_o = -10 cm.

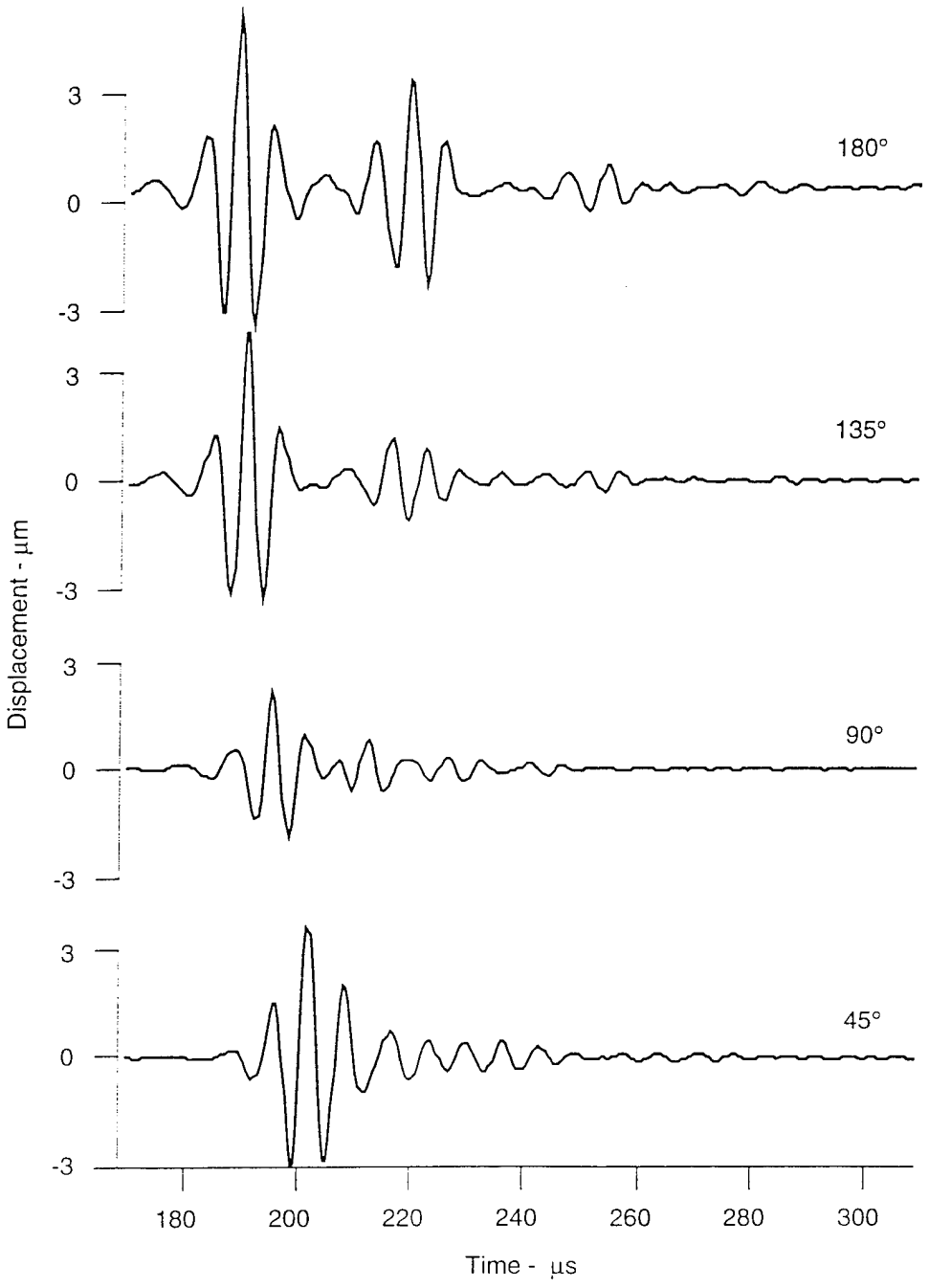

Figure 5.2
Angular dependence of scattered fast wave.

return at different angles was consistent with refraction of the plane wave through the sphere with a longitudinal wave speed of 6001 m/s. Likewise, the time difference between the specular return and the successive Rayleigh waves was consistent with a wave moving around the circumference of the sphere with a transverse wave speed of 3208 m/s.

6. EXPERIMENTAL RESULTS

At present, experimental comparisons for the full angular spread of predictions given in Figs. 5.1 and 5.2 are not available. However, both experimental measurements and numerical data were obtained for the forward scattering case (0°).

The experiments were conducted in a glass aquarium filled with sand and water. The aquarium was 25 cm wide, 51 cm long, and 30 cm deep. It was filled to a depth of 20 cm with a sand and water mixture, with an additional 6 cm of water above. Trapped air bubbles were coaxed from the sand using water circulation pumps and a vacuum chamber. With the circulation pumps in the water, the aquarium was placed in the vacuum chamber and the pressure was reduced to 0.06 atm. The circulation pumps were then turned on for 3-4 h, enhancing the coalescence and removal of air bubbles. Afterwards, the pumps were turned off and the aquarium remained under vacuum overnight, allowing more trapped air to escape. Next, the aquarium was removed from the vacuum chamber, and the source, target, and receiver assembly were inserted into the sand very carefully, in the configuration shown in Fig. 6.1. The sand was then encouraged to settle by placing the filled aquarium on a platform vibrating with a very small vertical amplitude at a frequency of 58 Hz for 10 min. The aquarium and vibrating platform are shown in Fig. 6.2. Finally, the entire apparatus was placed back in the vacuum chamber, and the pressure was reduced to 0.06 atm. Measurements were not taken until the apparatus had been under vacuum for an additional 2 h, allowing more air bubbles to escape from the sediment.

The total assembly, shown in Fig. 6.3, was designed to maintain equal depths for each of the three elements. The steel rod supporting the target was 0.6 cm in diameter at the rod/target interface. The steel sphere target was 3.5 cm in diameter. The sound source and receiver are wideband transducers constructed of a new composite material containing piezoelectric particles in a rubber matrix. The assembly was engineered so that the distances between the source and target and between the target and receiver were adjustable, as was the angle between the source, target, and receiver. It is capable of measuring

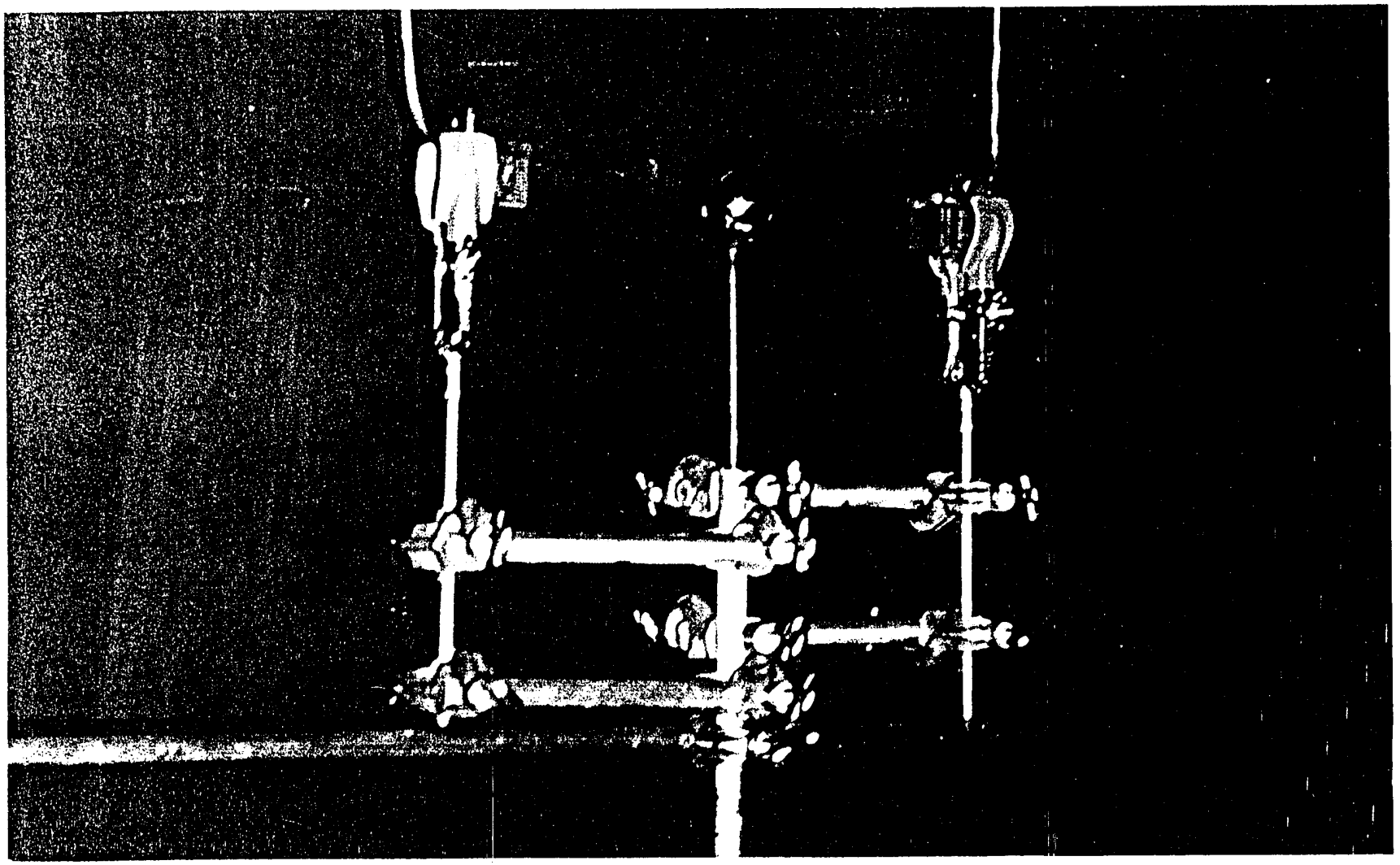

Figure 6.1
Photograph of experimental source, target, and receiver assembly.

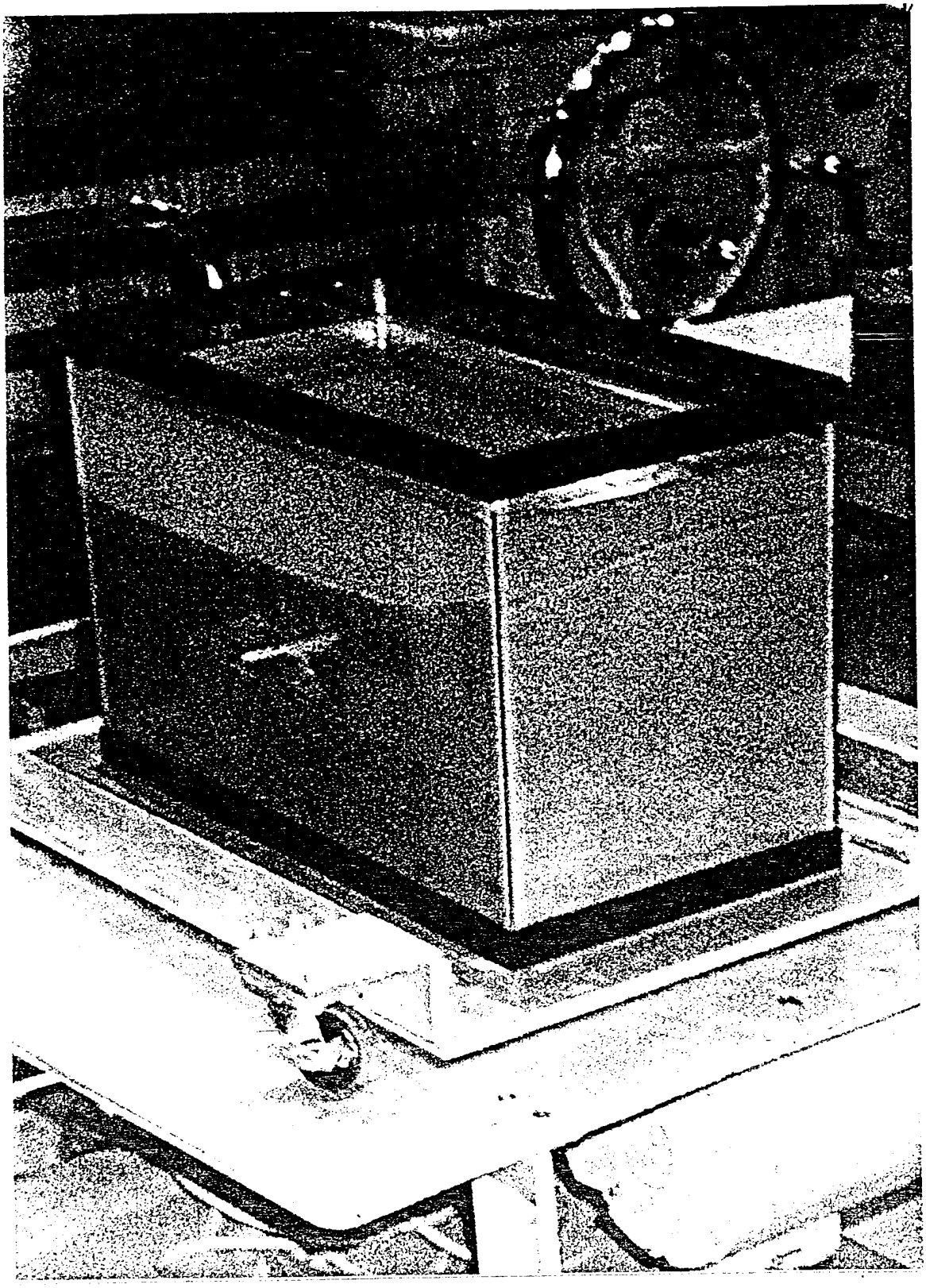

Figure 6.2
Photograph of aquarium and vibrating platform.

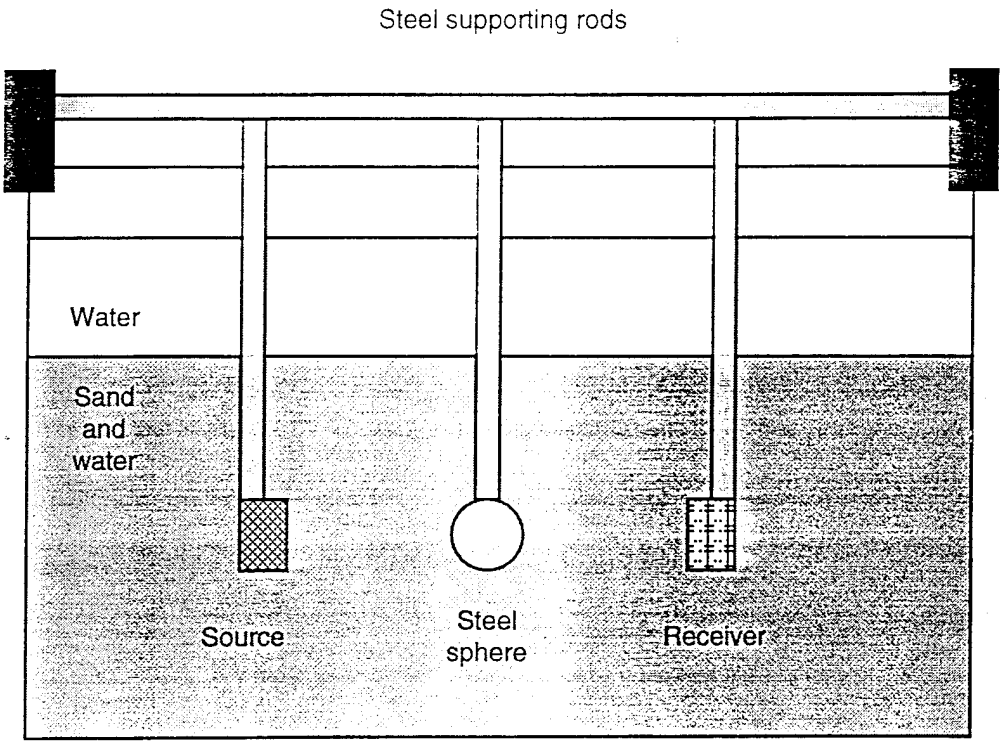

Figure 6.3
A cross-sectional schematic of the experimental apparatus.

scattered signals as a function of the bistatic angle θ, as shown in Fig. 6.4. The experiment reported here used $\theta = 0°$.

Two sets of measurements were taken -- one with a spherical target, in water-saturated sand, and the other with no target, in water. In both cases, the distance between the faces of the source and receiver transducers was 20 cm. When used, the target was midway between the two transducers. The measured data consisted of the input current of the source transducer and the output voltage of the receiver transducer. The data were processed by first filtering out the (very small) dc component and then tapering the trailing end of the signal to compensate for periodic mismatch. These processed data were then Fourier transformed, and the transfer functions were calculated via a Wiener filter.

The transfer function for the case of no target in water was used to deconvolve the transducer response from the data for the case of a spherical target in water-saturated sand. The process used assumes the system is linear. The transfer function for the no-target case represents the unobstructed response of the transducers in an essentially lossless medium (water), relative to water-saturated sand. However, it does include a spreading loss which is inversely proportional to the square of the separation between the two transducers. This loss was divided out of the no-target transfer function, giving the transfer function due solely to the transducer response. This, in turn, was divided out of the transfer function for the case of a spherical target in water-saturated sand, via a Wiener filter. The result, assuming the system is linear, was the experimental transfer function from input pressure to output pressure for a spherical steel target in water saturated sand.

The same transfer function was simulated numerically, and the power spectrum of the simulation was compared to the experimental power spectrum. To account for the narrower frequency range of the simulated incident wave, both transfer functions were passed through a 50-250 kHz raised cosine filter prior to calculating the power spectra. The result is shown in Fig. 6.5.

As shown by the difference spectrum in Fig. 6.5, the two power spectra agree to within ±10 dB at all frequencies. However, the structure of the two

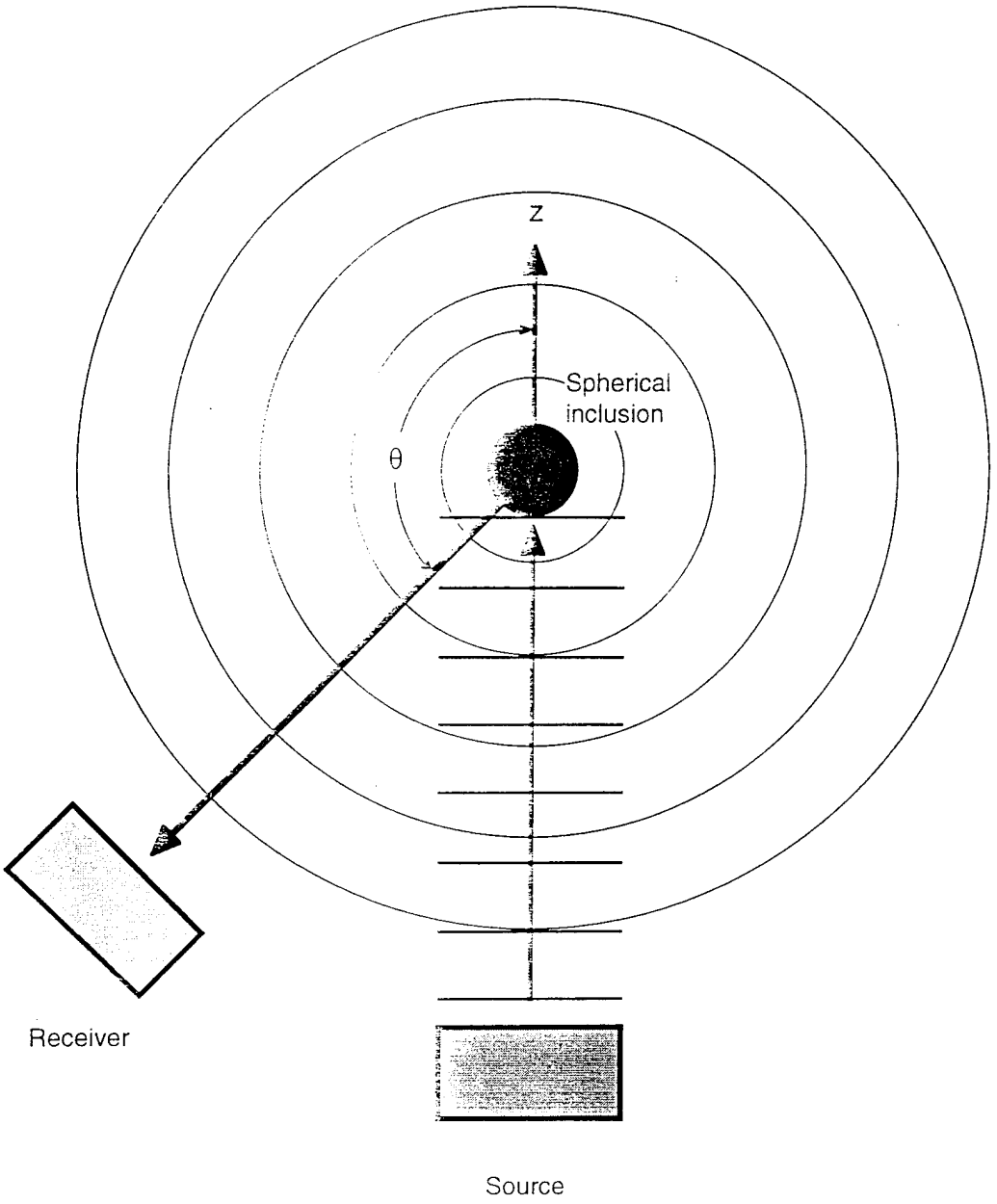

Figure 6.4
Plan view of target, source, and receiver geometry.

ARL - UT
AS-95-1240
DJY/RFO
12-95/svr

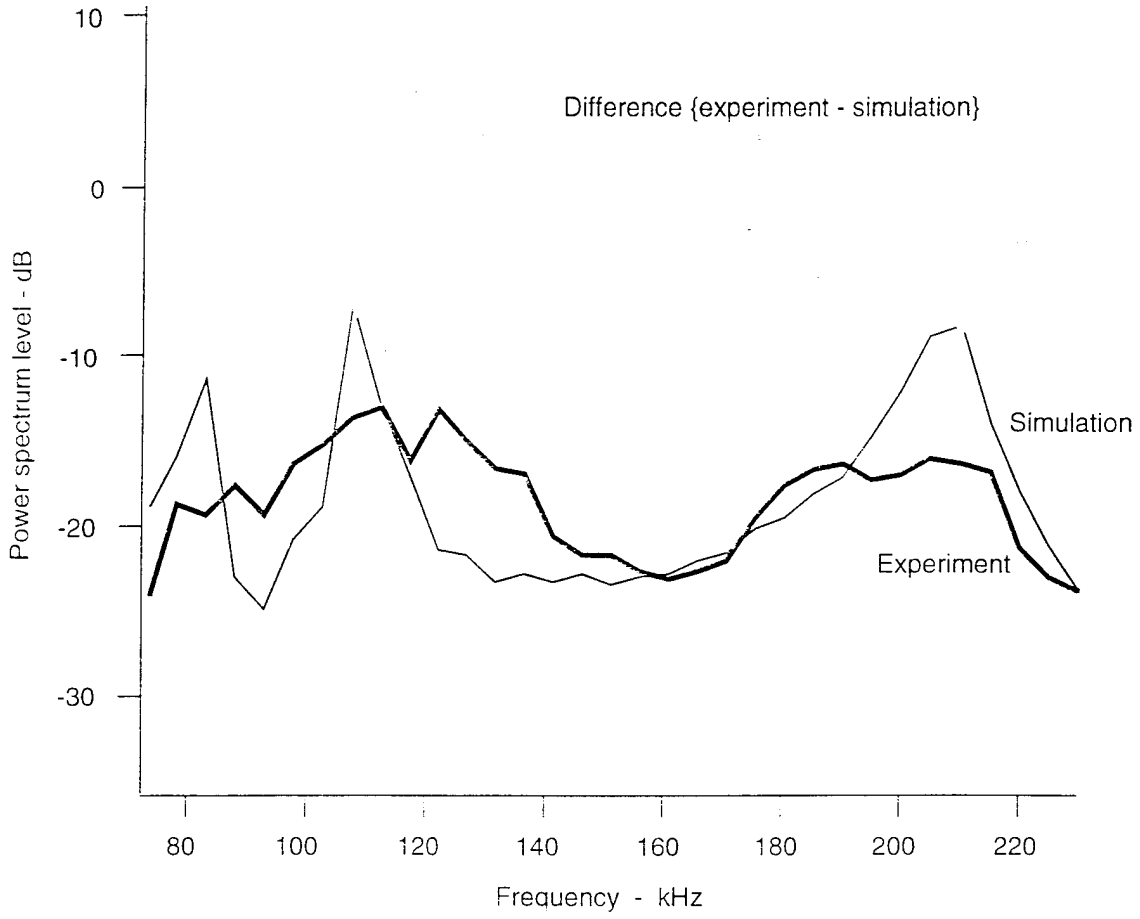

Figure 6.5
Comparison of the experimental and simulated power spectral responses in the case of forward scattering (0°).

spectra are notably different. The simulated spectrum has prominent, closely spaced peaks at 83 kHz and 107 kHz, and a third prominent peak at 207 kHz, whereas the experimental spectrum only has two large bumps. The bumps do, however, correspond roughly to the peaks in the simulated spectrum. The larger bump overlaps the two closely spaced peaks, and the smaller bump overlaps the third peak.

A comparison of the bandlimited impulse responses of theoretical model and experiment is shown in Fig. 6.6. It indicates that there is much similarity in the initial part of scattered pulse. The main difference is that the model predicts a more persistent ringing than the experimental data, indicating that the experimental system is more heavily damped. Possible reasons include (1) imperfections in the coupling between tangential motion at the surface of the sphere and the surrounding sand, resulting in greater damping in the Rayleigh wave response than predicted, and (2) distortion caused by the weld between sphere and mounting rod.

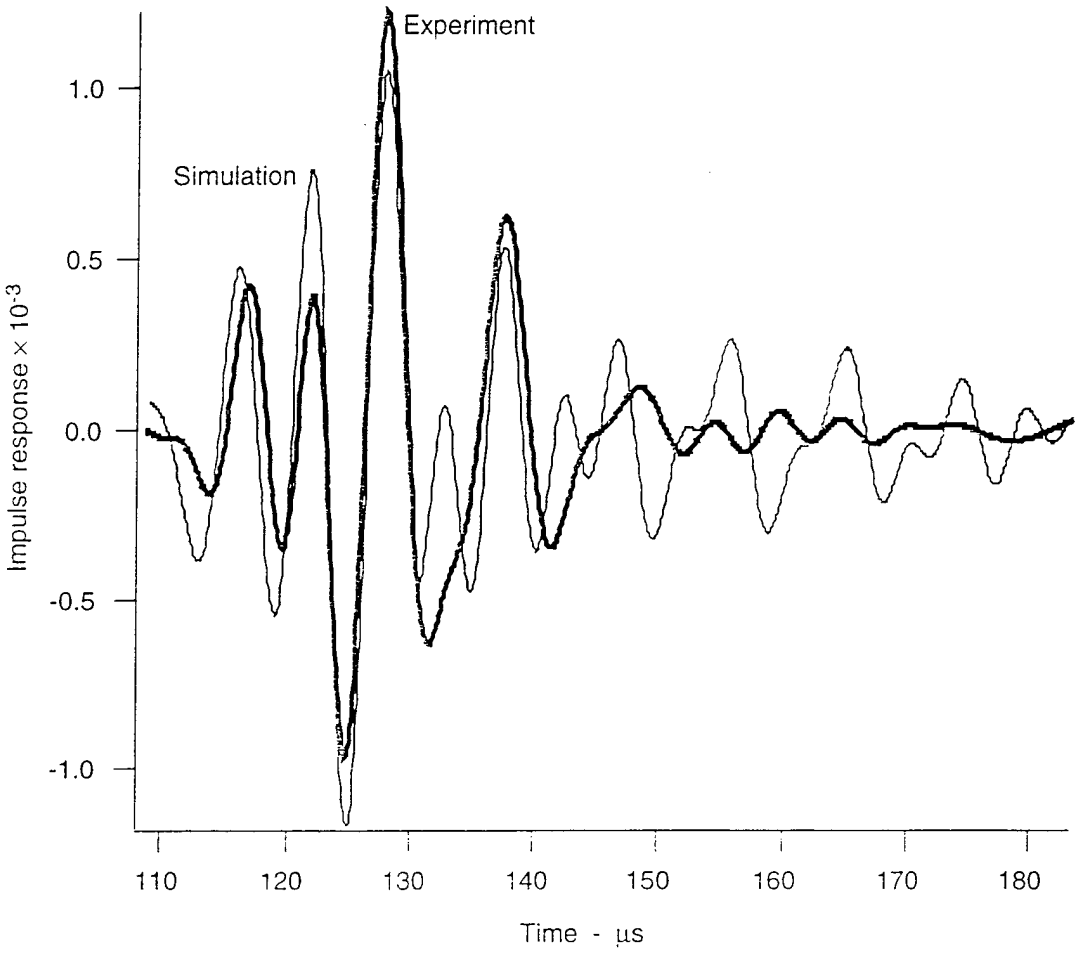

Figure 6.6
Comparison of the experimental and simulated impulse responses in the case of forward scattering (0°).

This page intentionally left blank.

7. CONCLUSIONS

The results in Figs. 5.2 and 5.3 demonstrate very significant differences in the behavior of the scattered Biot fast and slow waves. This diversity guarantees there will be notable discrepancies between the scattering predictions of a Biot sediment model and an elastic sediment model, since the latter is inherently incapable of manifesting such diversity. If borne out experimentally, the strongly backscattered first Rayleigh wave in the slow wave spectrum could be a significant resource for the long range detection of targets buried in the seabed. By the principle of reciprocity, this signal return would register most strongly at the source of the incident wave, i.e., at the location of the active sonar used to scan the sediment. This is the most advantageous condition for self-contained target detection. Further simulations and experiments are required to determine the relative differential scattering cross sections for incident fast versus slow waves.

The forward scattering simulation result, depicted in Figs. 6.5 and 6.6, are in good qualitative agreement with the experimental measurements. The simulated signal strength is closely centered on the experimental signal strength, and the coarse grain features of the two spectra are similar. However, there are notable differences on a finer scale. The two closely spaced peaks in the simulated power spectrum were not resolved experimentally. The reason for this is unclear, but there are several possibilities. One is imperfections in the coupling between tangential motion at the surface of the sphere and the surrounding sand, resulting in greater damping in the Rayleigh wave response than predicted. Another is that the target support rod interfered with the experimental resolution of the two peaks. Further experimentation is required to determine whether one of these, or some other, explanation is correct.

This page intentionally left blank.

ACKNOWLEDGMENTS

We are very grateful to Adrienne Mautner, of The University of Texas at Austin, who helped with the experimental procedure. We also wish to thank Justin Beres, of The University of Texas at Austin, who is responsible for much of the preliminary code development for this project.

This page intentionally left blank.

REFERENCES

1. P. C. Hines, "Theoretical Model of Acoustic Backscatter from a Smooth Seabed," J. Acoust. Soc. Am. 88(1), 324-334 (1990).

2. D. K. Dacol and D. H. Berman, "Sound Scattering from a Randomly Rough Fluid-Solid Interface," J. Acoust. Soc. Am. 84(1), 292-302 (1988).

3. M. Stern, A. Bedford, and H. R. Millwater, "Wave Reflection from a Sediment Layer with Depth-Dependent Properties," J. Acoust. Soc. Am. 77(5), 1781-1788 (1985).

4. N. P. Chotiros, "Biot Model of Sound Propagation in Water-Saturated Sand," J. Acoust. Soc. Am. 97(1), 199-214 (1995).

5. N. P. Chotiros, "High Frequency Bottom Penetration: Panama City Experiment Analysis III," Applied Research Laboratories Technical Report No. 91-18 (ARL-TR-91-18), Applied Research Laboratories, The University of Texas at Austin, 1991.

6. N. P. Chotiros, "High Frequency Acoustic Penetration Analysis," Applied Research Laboratories Technical Report No. 89-28 (ARL-TR-89-28), Applied Research Laboratories, The University of Texas at Austin, May 1989.

7. M. A. Biot, "Theory of Propagation of Elastic Waves in a Fluid-Saturated Porous Solid, I. Low-Frequency Range," J. Acoust. Soc. Am. 28, 168-178 (1956).

8. M. A. Biot, "Theory of Propagation of Elastic Waves in a Fluid-Saturated Porous Solid, II. Higher Frequency Range," J. Acoust. Soc. Am. 28, 179-191 (1956).

9. J. G. Berryman, "Scattering by a Spherical Inhomogeneity in a Fluid-Saturated Porous Medium," J. Math. Phys. 26, 1408 (1985).

10. S. Kargl and R. Lim, "A Transition Matrix Formalism for Scattering in Homogeneous, Saturated, Porous Media," J. Acoust. Soc. Am. 94(3), 1527-1550 (1993).

11. C. Zimmerman and M. Stern. "Scattering of Plane Compressional Waves by Spherical Inclusions in a Poroelastic Medium," J. Acoust. Soc. Am. 94(1), 527-536 (1993).

12. P. M. Morse and H. Feshbach. *Methods of Theoretical Physics* (McGraw-Hill Book Company, Inc., New York, 1953).

13. C. F. Ying and R. Truell, "Scattering of a Plane Longitudinal Wave by a Spherical Obstacle in an Isotropically Elastic Solid," J. Appl. Phys. 27, 1086 (1956).

14. Y. H. Pao and C. C. Mow, "Scattering of Plane Compressional Waves by a Spherical Obstacle," J. Appl. Phys. 34, 493 (1963).

26 October 1995

DISTRIBUTION LIST
ARL-TR-95-32
Final Report under Contract N00039-91-C-0082,
TD No. 01A2081, Buried Target Detection Model

Copy No.	
	Commanding Officer Naval Research Laboratory Stennis Space Center, MS 39529-5004
1 - 3	Attn: D. Ramsdale (Code 7170)
4	D. Lott (Code 7431)
5	E. Franchi (Code 7100)
6	S. Tooma (Code 7430)
7	S. Stanic (Code 7174)
8	M. Richardson (Code ~~431~~ 7431)
9	R. Meredith (Code 7174)
10	Library (Code 7032.2)
	Office of Naval Research San Diego Regional Office 4520 Executive Drive, Suite 300 San Diego, CA 92121-3019
11	Attn: J. Starcher, ACO
	Director Naval Research Laboratory Washington, DC 20375
12	Attn: Code ~~2627~~ 5227
13	B. Houston (Code ~~5136~~) 7130
	DTIC-OCC Defense Technical Information Center 8725 John J. Kingman Road, Suite 0944 Fort Belvoir, VA 22060-6218
14 - 25	Attn: Library
	Director Research Program Department Office of Naval Research Ballston Tower One 800 North Quincy Street Arlington, VA 22217-5000
26	Attn: J. Simmen (Code 321)
27	E. Chaika (Code 322)
28	W. Ching (Code 321)
29	T. Goldsberry (Code 322)
30	~~D. Houser (Code 333)~~ retired

Distribution List for ARL-TR-95-32 under Contract N00039-91-C-0082, TD No. 01A2081 (cont'd)

Copy No.

	Commander Naval Meteorology and Oceanography Command Stennis Space Center, MS 39522-5000
31	Attn: D. Durham (N5A)
32	R. Martin (N5C)
	Commander Program Executive Office - Mine Warfare Crystal Plaza Bldg 6 2531 Jefferson Davis Highway Arlington, VA 22242-5167
33	Attn: J. Grembi (PEOMIW)
34	D. Gaarde (PMO407B)
	G & C Systems Manager MK48/ADCAP Program Office National Center 2 2521 Jefferson Davis Hwy. 12W32 Arlington, VA 22202
35	Attn: H. Grunin (PMO402E1)
	Program Manager MK50 Torpedo Program Office Crystal Park 1 2011 Crystal Drive, Suite 1102 Arlington, VA 22202
36	Attn: A. Knobler (PMO406B)
	Commander Dahlgren Division Naval Surface Warfare Center Dahlgren, VA 22448-5000
37	Attn: Library
	Commander Dahlgren Division Naval Surface Warfare Center Silver Spring, MD 20903-5000
38	Attn: S. Martin (G94)
39	J. Sherman (N50)
40	M. Stripling (N04W)

Distribution List for ARL-TR-95-32 under Contract N00039-91-C-0082, TD No. 01A2081 (cont'd)

Copy No.

Director
Applied Physics Laboratory
The University of Washington
1013 NE 40th Street
Seattle, WA 98105
41 Attn: R. Spindel
42 D. Jackson
43 K. Williams
44 S. Kargl

Director
Life Sciences Directorate
Office of Naval Research
Arlington, VA 22217-5000
45 Attn: S. Zornetzer (Code 114)

Director
Marine Physical Laboratory
The University of California, San Diego
San Diego, CA 92152
46 Attn: K. Watson
47 C. de Moustier

Commander
Mine Warfare Command
325 Fifth St., SE
Corpus Christi, TX 78419-5032
48 Attn: G. Pollitt (N02R)

Applied Research Laboratory
The Pennsylvania State University
P.O. Box 30
State College, PA 16804-0030
49 Attn: L. Hettche
50 R. Goodman
51 E. Liszka
52 D. McCammon
53 F. Symons
54 Library

Distribution List for ARL-TR-95-32 under Contract N00039-91-C-0082, TD No. 01A2081 (cont'd)

Copy No.

National Center for Physical Acoustics
University of Mississippi
Coliseum Drive
University, MS 38677
55 Attn: J. Sabatier

Commanding Officer
Coastal Systems Station, Dahlgren Division
Naval Surface Warfare Center
Panama City, FL 32407-5000
56 Attn: M. Hauser (Code 10CD)
57 R. Lim (Code 130B)
58 E. Linsenmeyer (Code 10P)
59 D. Todoroff (Code 130)

Commander
Naval Undersea Warfare Center Division
New London, CT 06320-5594
60 Attn: J. Chester (Code 3112)
61 P. Koenig (Code 33A)

Advanced Research Projects Agency
3701 North Fairfax Drive
Arlington, VA 22203-1714
62 Attn: W. Carey

Commander
Naval Undersea Warfare Center Division
Newport, RI 02841-5047
63 Attn: J. Kelly (Code 821)
64 F. Aidala (Code 842)
65 W. Gozdz (Code 843)

Physics Department
The University of Texas at Austin
Austin, TX 78712
66 Attn: T. Griffy

Aerospace Engineering Department
The University of Texas at Austin
Austin, TX 78712
67 Attn: M. Bedford
68 M. Stern

Distribution List for ARL-TR-95-32 under Contract N00039-91-C-0082, TD No. 01A2081 (cont'd)

Copy No.	
69	Robert A. Altenburg, ARL:UT
70	Hollis Boehme, ARL:UT
71	Frank A. Boyle, ARL:UT
72	Nicholas P. Chotiros, ARL:UT
73	John M. Huckabay, ARL:UT
74	Thomas G. Muir, ARL:UT
75	Dennis J. Yelton, ARL:UT
76	Library, ARL:UT
77 - 81	Reserve, ARL:UT

REPORT DOCUMENTATION PAGE

Form Approved
OMB No. 0704-0188

1. AGENCY USE ONLY (Leave blank)	2. REPORT DATE	3. REPORT TYPE AND DATES COVERED
	26 Oct 95	final 21 Jun 94 - 30 Jun 95

4. TITLE AND SUBTITLE

Scattering of a Transient Plane Compression Wave by a Spherical Inclusion in a Biot Medium, Final Report under Contract N00039-91-C-0082, TD No. 01A2081, Buried Target Detection Model

5. FUNDING NUMBERS

N00039-91-C-0082,
TD No. 01A2081

6. AUTHOR(S)

Yelton, Dennis J. Stern, Morris Schantz, Hans G.

7. PERFORMING ORGANIZATION NAMES(S) AND ADDRESS(ES)

Applied Research Laboratories
The University of Texas at Austin
P.O. Box 8029
Austin, Texas 78713-8029

8. PERFORMING ORGANIZATION REPORT NUMBER

ARL-TR-95-32

9. SPONSORING/MONITORING AGENCY NAME(S) AND ADDRESS(ES)

Naval Research Laboratory
Stennis Space Center, MS 39529-5004

Space and Naval Warfare Systems Command
Department of the Navy
Arlington, VA 22245-5200

10. SPONSORING/MONITORING AGENCY REPORT NUMBER

NRL/CR/7170--96-0006

11. SUPPLEMENTARY NOTES

12a. DISTRIBUTION/AVAILABILITY STATEMENT

Approved for public release; distribution is unlimited.

12b. DISTRIBUTION CODE

13. ABSTRACT (Maximum 200 words)

The scattering of an arbitrary transient plane wave by a spherical inclusion in a Biot medium is modeled, by applying the single frequency steady-state solution of Zimmerman and Stern to the discrete Fourier components of the transient signal, and assuming linear superposition. The solution of Zimmerman and Stern is an analytical series solution. Its accuracy is mainly determined by computation errors and the convergence of the series. The incident pulse can be any combination of Biot fast and slow waves. The theoretical results for certain cases are shown. They are also compared to experimental measurements. This work is an integral part of an effort to model the acoustic response of buried objects in the ocean sediment.

14. SUBJECT TERMS

Biot, buried, inclusion, porous, sand, sediment, sphere

15. NUMBER OF PAGES

37

16. PRICE CODE

17. SECURITY CLASSIFICATION OF REPORT	18. SECURITY CLASSIFICATION OF THIS PAGE	19. SECURITY CLASSIFICATION OF ABSTRACT	20. LIMITATION OF ABSTRACT
UNCLASSIFIED	UNCLASSIFIED	UNCLASSIFIED	SAR

NSN 7540-01-280-5500

Standard Form 298 (Rev. 2-89)
Prescribed by ANSI Std. 239-18
298-102